LA-UR-18-31644
Approved for public release; distribution is unlimited.

Title: Segmented scintillators for megavolt radiography

Author(s): Winch, Nicola M.
Watson, Scott Avery
Hunter, James F.

Intended for: IEEE Nuclear Science Symposium and Medical Imaging Conference, 2018-11-10 (Sydney, Australia)

Issued: 2018-12-13

Segmented scintillators for megavolt radiography

N. M. Winch, S. A. Watson, and J. F. Hunter
Los Alamos National Laboratory, Los Alamos, NM 87545
Email: nwinch@lanl.gov

***Abstract*—In megavolt radiography the detection efficiency of conventional detectors is low due to the small interaction probability of the high energy radiation. Segmented scintillators improve the efficiency of detector systems mainly through an increased density. Various segmented scintillators have been compared to a commercial powdered scintillator screen in terms of their modultion transfer function, noise power spectra and detective quantum efficiency. A 50 $\pm$ 9% DQE system was demonstrated with segmented BGO and a room temperature lens-coupled camera for the first time. A lower cost but lower density alternative, a glass fiber optic faceplate, has an efficiency of 30 $\pm$ 7%.**

I. Introduction

Due to the high penetrating power of megavolt (MeV) radiation, MeV radiography is an effective way to image thick and/or dense objects [1]–[3]. Applications of MeV radiography include: radiation therapy, weld inspection, border security inspection of large cargo containers, flash radiography and non-destructive testing. One important problem of megavolt radiography is the low detection efficiency of the detector which makes cost effective radiographic systems difficult to construct. In addition, high efficiency detectors are required for applications where the radiation source has low flux, fast acquisition times are required and/or a very high quality image is needed.

The detective quantum efficiency (DQE) of a system can be increased by using thick, high density, segmented scintillators. Segmented scintillators are a good choice for many applications, but they are often not implemented due to their high cost, and lack of commercial availability.

Segmented scintillators are composed of individual pixel light pipes which improve the DQE as they can be made much thicker than powdered scintillators (e.g. gadolinium oxysulfide, Gd_2O_2S), and produce a planar image suitable for imaging with lens-coupled cameras [4]. One such scintillator is a metal matrix filled with scintillator pixels, combining the stopping power of a high-Z, high-density material with the light output of a scintillator [5]. This combination also allows for isolation of the optical scatter. A lower density but lower cost alternative is a scintillating fiber optic glass faceplate which consists of bundles of scintillating glass fibers fused together.

The imaging perforance of various segmented scintillators has been investigated in terms of their resolution, noise power and detective quantum efficiency.

II. Simulations

Monte Carlo simulations were used to investigate the resolution and energy deposited in scintillators as a function of incident photon energy, thickness and density. The scintillator is an IQI terbium activated silicate glass (density of 3.8 g/cm^3) [6], [7], referred to as "glass" in this study. The 2D CYLTRAN package from the Integrated Tiger Series (ITS) electron/photon transport codes [8] was used. Simulations were run with a 5 μm step size for a total radial zone of 10 mm. 50 million mono-energetic photons in the energy range 1 - 20 MeV generated from a point source were followed. Typical run times were between 30s and 30 minutes on an Intel Xeon 3.10 GHz CPU with 16 GB RAM. The ITS output produces a file of energy deposited in each segment, which is analogous to the point spread function (PSF) of the detector, and is used to determine the modulation transfer function (MTF). Details of this conversion have been published previously [9].

Fig.1 shows the resolution at 50% MTF and energy deposited in the various thickness glass scintillators as a function of incident photon energy. In general the resolution decreases as the photon energy is increased, because of the increase in multiple scattering events with higher energies. For thin scintillators (e.g. the 5 mm thick scintillator) the resolution initially decreases with increasing photon energy, until $\sim$5 MeV when the resolution increases with a further increase in photon energy. This latter increase in resolution is caused by higher energy photons having a narrower scattering angle which leads to single scattering events becoming dominant (see Winch et. al. [9]). As expected, the energy deposited in the scintillator increases with both increasing thickness and increasing photon energy.

A 10 mm thick tungsten and glass segmented scintillator was simulated as a homogenous mixture with the glass weight fraction varied between 25% (density of 15.4 g/cm^3) and 100%. Fig.2 shows the resolution at 50% MTF and energy deposited in the various weight fraction segmented scintillators as a function of photon energy. Increasing the tungsten weight fraction increases the resolution as a result of the high-density tungsten decreasing the spread of the long-range photons. The energy deposited also increases with the increased fraction of tungsten, due to the higher stopping power of the tungsten. However, these results cannot be used to infer the sensitivity of the detector as the energy deposited in the tungsten does not directly produce the output light that is recorded. The heterogeneous nature of this structure at scales of interest was one major reason for this test campaign.

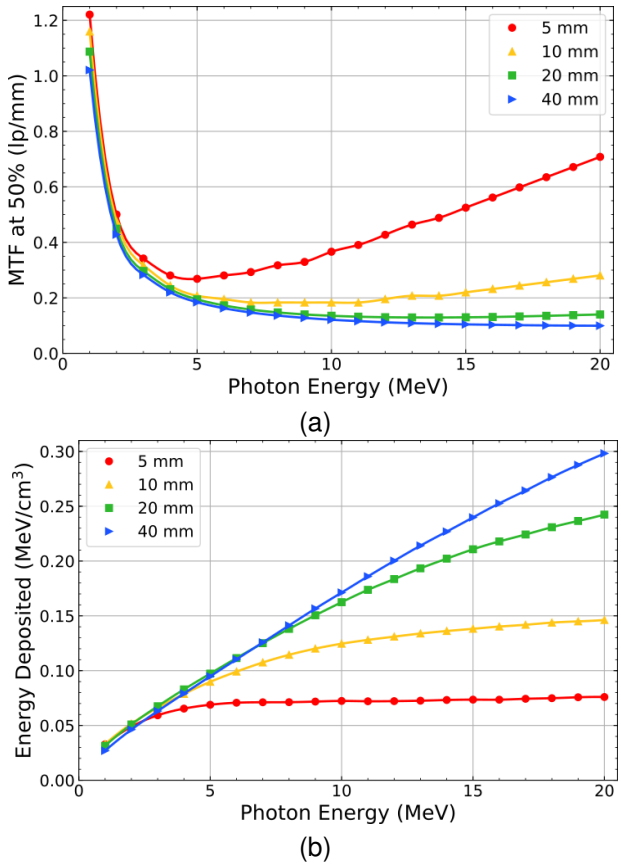

Fig. 1. (a) Resolution at 50% MTF and (b) energy deposited for various thicknesses of glass as a function of incident photon energy.

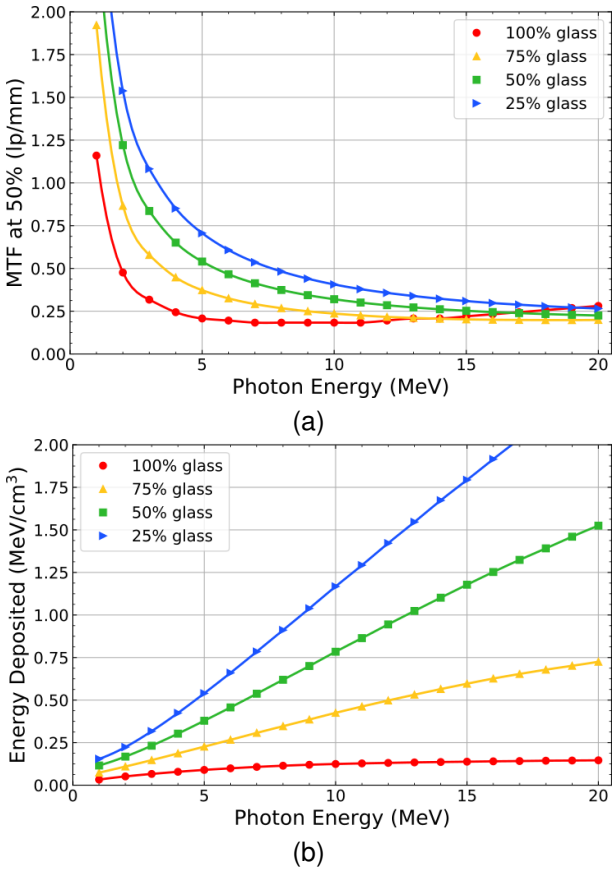

Fig. 2. (a) Resolution at 50% MTF and (b) energy deposited for various homogenous mixtures of tungsten and glass as a function of incident photon energy.

III. Experimental Setup

The MTF, noise power spectrum (NPS) and detective quantum efficiency (DQE) of various segmented scintillators was experimentally investigated. The source was a 2.4 Curie cobalt-60 (Co-60) source which equally produces 1.17 and 1.33 MeV gamma rays. The Co-60 source was placed 600 - 900 mm from the scintillator which in turn was placed 200 mm from the camera (see Fig.3). The camera used was a Nikon Df, SLR camera with an 85 mm, f1.4 lens with a +2 diopter to decrease the focusing distance without impacting the f# [2].

Three segmented scintillators were investigated, a segmented bismuth germinate (BGO) scintillator, an IQI fiber optic glass scintillator and a custom tungsten-glass grid. These were compared to a commercially available gadolinium oxysulfide, "DRZ high", scintillator. The properties of the scintillators are shown in Table I.

Fig.4a shows an example of a 250 μm pixel pitch glass fiber optic faceplate under UV illumination (sample provided by Schott glass). The individual fibers and the hexagon structure of the fiber bundles can be clearly seen.

The tungsten-glass grid schematic is shown in Fig.4b. The dimensions (L x W x H) of the grid are 400 mm x 40 mm x 10 mm with almost 200,000 individual glass fiber locations. The tungsten grid is made by etching the hole pattern in individual layers, and gluing the stacked layers together. The effective

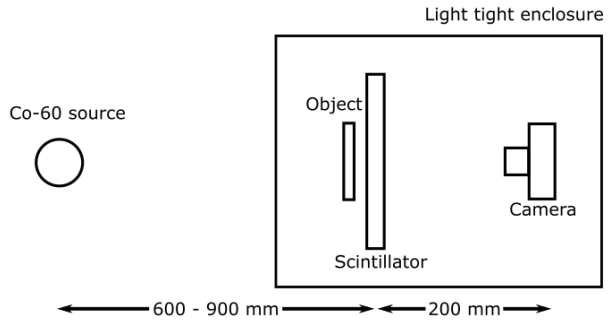

Fig. 3. Experimental setup for testing the various scintillators. (need to put dimensions on it)

pixel pitch of the tungsten-glass grid is 400 μm, with a hole diameter of 300 μm and a glass fiber diameter of ~250 μm.

IV. Results

Instead of measured MTFs which are sampled, and aliased, a calculated pre-sampled MTF [10] was used. The simulations have been shown to accurately predict system MTF in previous work [9]. The MTFs have been adjusted for the spot size of the Co-60 source (5 mm diameter) [11] and for the optical scatter for the DRZ high scintillator [12].

TABLE I
PROPERTIES OF SCINTILLATORS INVESTIGATED IN THIS STUDY.

Scintillator	Thickness	Pixel pitch	Density (g/cm^3)	Line of sight mass (g/cm^2)	DQE theory (%)	DQE measured (%)
BGO	20 mm	1.1 mm	6.7	14.2	54	50 $\pm$ 9
IQI fiber optic faceplate	20 mm	20 μm	3.4	7.6	32	30 $\pm$ 7
Tungsten-glass grid	10 mm	400 μm	12.6	12.6	50 (10)[a]	2 $\pm$ 0.5
DRZ high	300 μm	n/a	4.7	0.14	1	1 $\pm$ 0.3

[a] 50% DQE assumes all incident γ-rays cause light output, which is not the case for γ-rays absorbed in the tungsten.

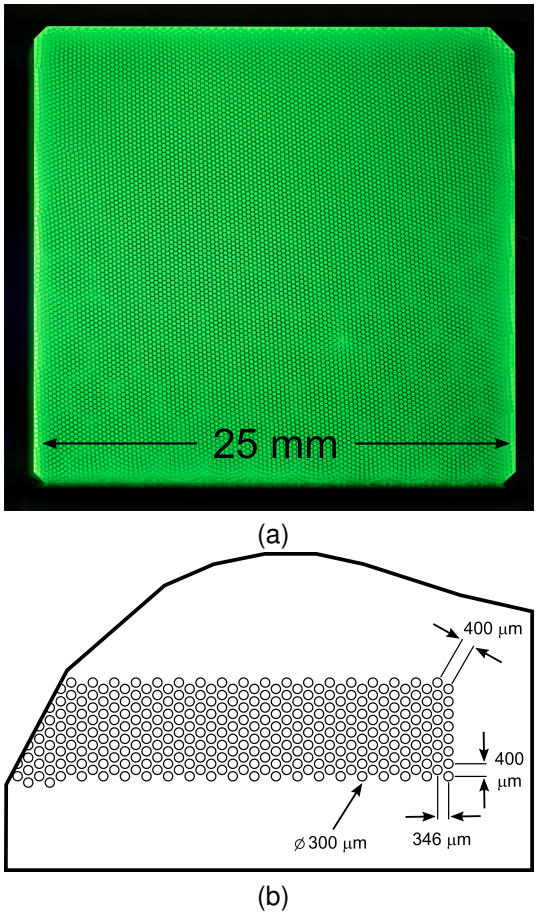

Fig. 4. (a) Example of a glass fiber optic faceplate with 250 μm fibers under UV illumination (sample provided by Schott). (b) Schematic showing the configuration of the tungsten-glass grid. (put the size of the faceplate on image - and on the schematic?)

The simulated MTFs are shown in Fig.5. The tungsten grid has the highest resolution because of the reduced scattering range of Compton scattered electrons and γ-rays. The DRZ plate has the lowest resolution which is counter to the thin scintillator results shown in Fig.1a. The low resolution for the DRZ plate is caused by the powdered nature of the scintillator causing large optical scatter and dominating the MTF.

The NPS of each scintillator was determined from two flat field images taken under the same conditions. The exposure time was 2 seconds for the BGO and IQI scintillators at a source to object distance of 900 mm. For the Gadox and tungsten-glass grid the exposure time was 4 seconds at a

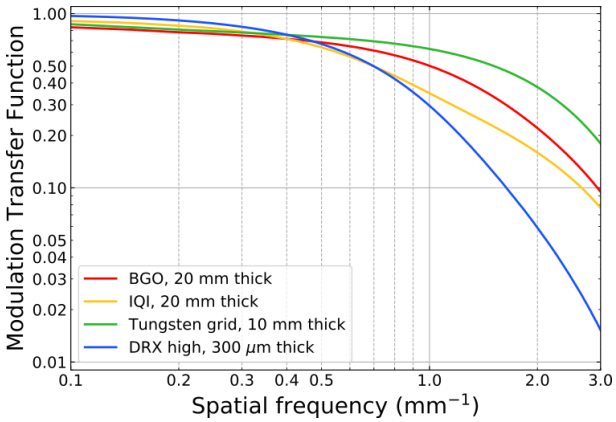

Fig. 5. Simulated MTFs of the scintillators studied. (Make the lines different? Fix DRX high)

distance of 600 mm. A region of interest of 1024 x 1024 pixels was selected and the ionization tracks of the γ-rays interaction with the camera CCD were removed by a statistical area replacement algorithm. The two flat fields were normalized to the mean pixel value and subtracted from each other. The resulting image is the noise image due to quantum mottle. The NPS was calculated from this noise image using the method of Hanson [13].

Fig.6 shows the NPS for the various scintillators, along with the associated Nyquist rates. The BGO segmented scintillator has the lowest noise, followed by the IQI fiber optic faceplate. The tungsten-glass grid has the highest noise which is relatively flat across all spatial frequencies. This white noise spectrum suggests that the light output is low and the system is not quantum limited [**?**].

The DQE as a function of spatial frequency is related to the MTF, NPS and the number of quanta (N_{eq}) incident on the scintillator and is expressed by,

$$DQE(f) = \frac{MTF^2(f)}{N_{eq} NPS(f)}. \quad (1)$$

The theoretical DQE for each scintillator, calculated as the fraction of 1.25 MeV γ-rays absorbed in the scintillator, is given in Table I. The theoretical DQE for the tungsten-glass grid ranges between $\sim$10-50% as the calculation assumes all incident γ-rays cause light output which is not the case for γ-rays absorbed in the tungsten.

The experimental DQEs for all the scintillators are shown in Fig.7. The BGO has a maximum DQE 50 $\pm$ 9%, which

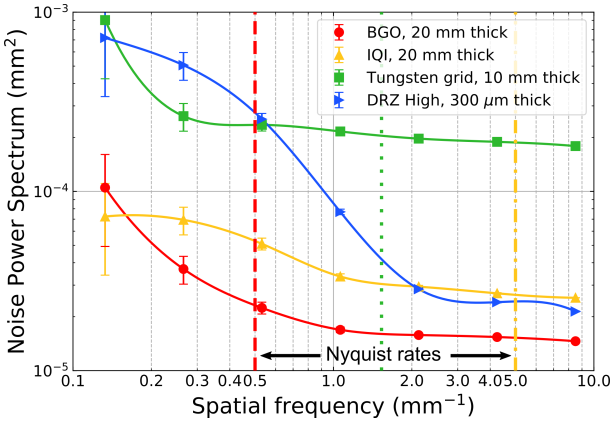

Fig. 6. NPS of the various scintillators as indicated. The vertical dashed lines show the Nyquist rates for the segmented scintillators.

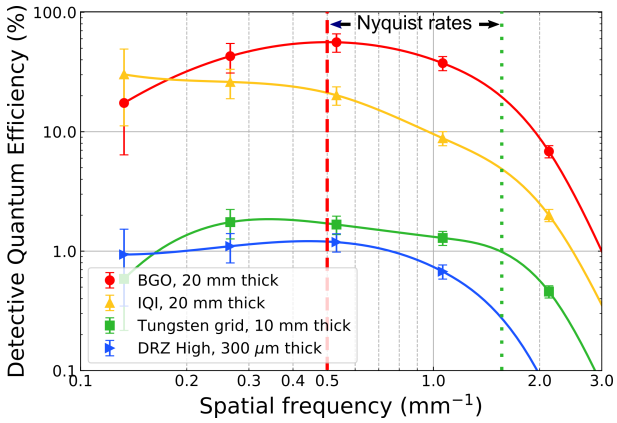

Fig. 7. DQE of the various scintillators as labeled. The vertical dashed lines show the Nyquist rates for the segmented scintillators.

agrees within uncertainties with both the theoretical value and the reported value [14]. The IQI fiber-optic faceplate has the next highest DQE with a maximum of 30 ± 7% and agrees within uncertainties to the theoretical value. The gadox has a DQE of 1 ± 0.3% as expected from a powder phosphor plate. The tungsten grid has a maximum DQE of 2 ± 0.5% which is a much lower DQE than expected due to the poor light transport and low energy absorption in the individual fibers creating a quantum-sink [15], [16].

V. Summary

Segmented scintillators improve the detective quantum efficiency of detector systems for high energy radiography. They do this by a combination of increased thickness, increased density and decreased scattering. The cost and performance trade-offs of such systems are driven by the overall density of the scintillator and the number of elements (e.g. polishing single crystal scintillators).

A 50% DQE system was demonstrated with segmented BGO and a room temperature camera for the first time. A low-cost camera and lens system does not require any cooling, and as such could be used for routine field operations. The glass fiber optic faceplate, with a DQE of 30%, is a good compromise between the expensive segmented BGO (or similar) scintillating crystals and commercial powdered scintillators. The tungsten-glass grid performed much lower than was expected and is likely due to the very low light output. The DQE is expected to improve at higher energy due to increased energy of primary particles (γ-rays).

Further work is underway to test these scintillators at higher energies (up to 20 MeV) and with Am-Si flat panels.

Acknowledgements

The authors would like to thank Collimated Holes, Bicron, Microsystems, and Schott North America.

References

[1] M. J. George, K. H. Mueller, R. H. O'Connor, and R. G. Schrandt, "The use of the Monte-carlo method to simulate high-energy radiography of dense objects," Los Alamos National Laboratory, Tech. Rep. LA-11727-MS, 1990.

[2] S. A. Watson, T. J. Kauppila, R. C. Haight, and K. H. Mueller, "Multiframe, high-energy, radiographic cameras for submicrosecond imaging," Los Alamos National Laboratory, Tech. Rep. LA-UR-95-3570, 1995.

[3] S. A. Watson, J. M. Gonzales, C. Gossein, M. D. Hoverson, A. Tubb, and M. D. Ulibarri, "Use of dense, monolithic, scintillator membranes as a high resolution imaging detector for megavolt radiography at U1-A and DARHT," Los Alamos National Laboratory, Tech. Rep. LA-UR-99-6491, 1999.

[4] S. A. Vasile, J. S. Gordon, M. B. Klugerman, V. V. Nagarkar, M. R. Squillante, G. Entine, S. A. Watson, and T. J. Kauppila, "Cost-effective segmented scintillating converters for hard x rays," pp. 2859 – 2859 – 8, 1996.

[5] S. A. Watson, "The DARHT camera," *Los Alamos Science*, vol. 28, 2003.

[6] R. A. Buchanan, C. Bueno, and H. Berger, "Terbium activated borate luminescent glasses coactivated with gadolinium oxide," U.S. Patent 5 108 959, 1992.

[7] H. Berger, D. Fry, M. Laux, and H. Malik, "Gamma and x-ray response of high density glass scintillators," in *IEEE Nuclear Science Symposium Conference Record*, vol. Fall Conference, 1994.

[8] B. C. Franke, R. P. Kensek, and T. W. Laub, "ITS version 6: The integrated TIGER series of coupled electron/photon Monte Carlo transport codes," Sandia National Laboratories, Tech. Rep. SAND2008-33311, 2008.

[9] N. M. Winch, S. A. Watson, and J. F. Hunter, "Modeling blur in various detector geometries for mev radiography," pp. 10 132 – 10 132 – 16, 2017.

[10] H. Fujita, D. . Tsai, T. Itoh, K. Doi, J. Morishita, K. Ueda, and A. Ohtsuka, "A simple method for determining the modulation transfer function in digital radiography," *IEEE Transactions on Medical Imaging*, vol. 11, no. 1, pp. 34–39, March 1992.

[11] C. Ekdahl, "Characterizing flash-radiography source spots," *J. Opt. Soc. Am. A*, vol. 28, pp. 2501–2509, 2011.

[12] M. O. LLC. Drz screens. [Online]. Available: http://www.mcio.com/Products/drz-screens.aspx

[13] K. M. Hanson, "Simplified method of estimating noise-power spectra," pp. 3336 – 3336 – 8, 1998.

[14] S. A. Watson, J. M. Gonzales, C. Gossein, M. D. Hoverson, and M. D. Ulibarri, "Quantum efficiency, noise power spectrum, linearity and sensitivity of the DARHT γ-ray camera," Los Alamos National Laboratory, Tech. Rep. LA-UR-00-653, 2000.

[15] I. A. Cunningham, "Degradation of the detective quantum efficiency due to a nonunity detector fill factor," pp. 3032 – 3032 – 10, 1997.

[16] J.-P. Bissonnette, I. A. Cunningham, D. A. Jaffray, A. Fenster, and P. Munro, "A quantum accounting and detective quantum efficiency analysis for video-based portal imaging," *Medical Physics*, vol. 24, no. 6, pp. 815–826, 1997.